



AMERICAN METEOROLOGICAL SOCIETY

Journal of Climate

EARLY ONLINE RELEASE

This is a preliminary PDF of the author-produced manuscript that has been peer-reviewed and accepted for publication. Since it is being posted so soon after acceptance, it has not yet been copyedited, formatted, or processed by AMS Publications. This preliminary version of the manuscript may be downloaded, distributed, and cited, but please be aware that there will be visual differences and possibly some content differences between this version and the final published version.

The DOI for this manuscript is doi: 10.1175/JCLI-D-11-00159.1

The final published version of this manuscript will replace the preliminary version at the above DOI once it is available.



Marine downscaling of a future climate scenario for Australian boundary currents

Chaojiao Sun¹
Ming Feng

Centre for Australian Weather and Climate Research, CSIRO Wealth from Oceans
National Research Flagship, Floreat, Western Australia, Australia

Richard J. Matear
Matthew A. Chamberlain
Peter Craig
Ken R. Ridgway
Andreas Schiller

Centre for Australian Weather and Climate Research, CSIRO Wealth from Oceans
National Research Flagship, Hobart, Tasmania, Australia

1

¹ *Corresponding author address:* Chaojiao Sun, CSIRO Marine and Atmospheric Research, Underwood Avenue, Floreat, WA 6014, Australia
E-mail: Chaojiao.Sun@csiro.au

ABSTRACT

Ocean boundary currents are poorly represented in existing coupled climate models, partly because of their insufficient resolution to resolve narrow jets. Therefore there is limited confidence in the simulated response of boundary currents to climate change by climate models. To address this issue, we use the eddy-resolving Ocean Forecasting Australia Model (OFAM), forced with bias-corrected output in the 2060s under SRES A1B from the CSIRO Mk3.5 climate model, to provide downscaled regional ocean projections. Mk3.5 captures a number of robust changes common to most climate models and are consistent with observed changes, including the weakening of the equatorial Pacific zonal wind stress and strengthening of the wind stress curl in the Southern Pacific, important for driving the boundary currents around Australia.

The 1990s climate is downscaled using air-sea fluxes from the ERA40 reanalysis. The current speed, seasonality, and volume transports of the Australian boundary currents show much greater fidelity to the observations in the downscaled model. Between the 1990s and the 2060s, the downsampling with the OFAM model simulates a 15% reduction in the LC transport, a 20% decrease in the ITF transport, a 12% increase in the EAC core transport, and a 35% increase in the EAC extension. The projected changes by the downsampling model are consistent with observed trends over the past several decades, and with changes in wind-driven circulation derived from Sverdrup dynamics. Although the direction of change projected from downsampling are usually in agreement with Mk3.5, there are important regional details and differences that will impact response of ecosystems to climate change.

1. Introduction

Ocean boundary currents are poorly represented in the current climate models that contribute to the Coupled Model Intercomparison Project (CMIP3), an initiative by the World Climate Research Programme (WCRP). This representation is partly due to insufficient horizontal resolution of about 1-2° (about 100-200 km) in the ocean component of climate models, too large to realistically simulate these narrow jets. As a result there is limited confidence in the structural changes in these boundary currents projected by climate models. However, the response of these currents to climate change may directly affect marine ecosystems and regional climate (e.g., Stock et al., 2011). Around Australia, both the eastern and western boundary currents flow poleward, bringing warm tropical water to the colder regions. The East Australian Current (EAC) is a relatively strong western boundary current with an annually averaged volume transport of 20-30 Sv ($1 \text{ Sv} \equiv 10^6 \text{ m}^3 \text{ s}^{-1}$) (Mata et al., 2000; Ridgway and Dunn, 2003). The Leeuwin Current (LC) is a narrow, weak eastern boundary current, with an annually averaged volume transport of ~3.4 Sv at 32°S (e.g., Feng et al., 2003). These currents are responsible for maintaining the marine ecosystems along the east and west coasts of Australia, both as a result of higher temperatures and alongshore dispersal (e.g. Booth et al., 2007; Lenanton et al., 2009).

As both the EAC and LC are primarily driven by large-scale wind forcing that are resolved by coarse-resolution climate models, more realistic simulations of the currents in a future climate could be obtained with an eddy-resolving ocean general circulation model using climate-model output as forcing. The present study uses the Ocean Forecasting Australia Model (OFAM; Oke et al., 2005) to downscale a future climate scenario from the CSIRO Mk3.5 climate model (Gordon et al., 2002).

Dynamical downscaling methods have been routinely applied to regional atmospheric circulation studies and hurricane simulations and projections (e.g., Emanuel 2006; Emanuel et al. 2008; Caldwell et al. 2009). However, there are relatively few studies of dynamical downscaling of ocean circulation for climate projections (e.g., Meier, 2006; Auad et al., 2006; Ådlandsvik and Bentsen, 2007; Ådlandsvik 2008). This study applies ocean dynamical downscaling to investigate the impact of climate change on the boundary currents in the Australian region. In Section 2, we present the models and forcing configurations for the downscaling experiments for two time periods, the 1990s and 2060s. In Section 3, we compare the downscaling results with the climate model projections, and discuss the changes between the two periods. In Section 4, we summarize and discuss the strengths and weaknesses of our ocean downscaling approach for climate change projections.

2. Methods

a. The models

The CSIRO Mk3.5 is one of the contributing CMIP3 climate models which informed the Fourth Assessment Report of the Intergovernmental Panel on Climate Change (IPCC AR4; Solomon et al., 2007). In Mk3.5, the ocean component is the Modular Ocean Model version 2 (MOM2) with a horizontal resolution of $1.875^{\circ} \times 0.933^{\circ}$ (Gordon et al., 2002). The Mk3.5 climate model is chosen in this study for the following reasons: (1) it is a model configured by CSIRO so we have ready access to both the developers and the forcing files; (2) it captures the average climate signals globally (Reichler and Kim, 2008) and in the southern hemisphere (Sen Gupta et al., 2009); (3) it simulates the teleconnection between the Indian and Pacific Ocean (Cai 2006). This teleconnection is the principal driving mechanism for the Leeuwin Current.

In this study, the bias-corrected atmospheric output from Mk3.5 model is used to force the OFAM (Oke et al., 2008) to simulate future ocean circulations. This approach is motivated by the understanding that most climate models have biases when simulating present climate. OFAM is based on the MOM4 ocean model (Griffies et al., 2005). While the domain is global, the resolution is enhanced to 10 km resolution in the greater Australian region (90°E-180°E, 72°S-16°N). Outside this domain, the horizontal resolution decreases to 0.9 degrees across the Pacific and Indian basins and to 2 degrees in the Atlantic Ocean. OFAM has 47 vertical levels, 35 of which are in the top 1000 m, and 20 in the top 200 m with 10-m resolution. OFAM is capable of simulating the current systems in the Australian region realistically, including their seasonal cycles and volume transports (e.g., Schiller et al., 2008). A major advantage of using OFAM for marine downscaling is its global configuration; there is no need to nest it inside a lower-resolution ocean model or apply open-boundary conditions. The disadvantage is higher computational costs compared to a regional-domain model.

b. Forcing configurations for downscaling

1) THE 1990S FORCING

To evaluate the downscaling approach and provide a reference state for interpreting results for the 2060s, a control experiment is run, forced by surface fluxes (heat, freshwater, and wind stress) derived from the ERA40 reanalysis (Uppala et al., 2005) in the 1990s. A repeat-year forcing dataset typical of average climatological conditions at the end of the 20th century is used to remove the complexity associated with interannual variability from external forcing. This was achieved by constructing a monthly climatology of air-sea fluxes based on the years 1993-2001 from ERA40. A correction to the heat and fresh water fluxes is added. This is calculated from an existing OFAM spin-up run for 1993-2001, forced by the ERA40 fluxes with the sea surface temperature (SST) and sea

surface salinity (SSS) weakly restored to observed values with a 30-day time scale. This ensures that the forcing applied does not cause the upper ocean state to drift. In addition, to account for daily variability, ERA40 daily anomalies from year 1995 are added (defined as the difference between daily values and monthly mean). The year of 1995, which is neither an El Niño nor La Niña year, is chosen as “normal”, to obtain daily variability independent of ENSO signals. To summarize, the forcing terms are:

$$\begin{aligned} \text{forcing (1990s)} = & \text{ERA40 monthly climatology (1993-2001)} + \text{ERA40 daily anomaly (1995)} + \\ & \text{flux correction (from 1993-2001 OFAM spin-up run)} \end{aligned} \quad (1)$$

The experiment with this repeat-year forcing is denoted “CTRL”. The initial condition is the December climatology from the OFAM spin-up run from 1993 to 2001 (Table 1).

2) THE 2060S FORCING

In CMIP3 present-climate simulations, large regional differences exist between the simulated surface fluxes of heat, freshwater and momentum and the observed fluxes (e.g., Sen Gupta et al., 2009). Figure 1 shows bias in zonal wind stress in four CMIP3 climate models compared with ERA40 analysis. The existence of biases in the CMIP3 climate models requires some thought when using these fluxes as forcing for OFAM. We hence employ a bias-correction technique, commonly used for atmospheric downscaling, to account for the surface flux biases of the Mk3.5 simulation. We take the difference of Mk3.5 surface fluxes between the decades of 2060s and 1990s and add it to present-day surface fluxes (used in the CTRL experiment) to produce bias-corrected surface fluxes for the 2060s. The Mk3.5 change in surface fluxes (heat, fresh water, and momentum fluxes) are from the SRES A1B simulation in the 2060s and the 20C3M simulation in the 1990s. A monthly climatology is computed from the monthly fields of Mk.35 output in the 1990s and 2060s to generate a repeat-year forcing

dataset similar to that in the CTRL experiment. This approach of generating the surface fluxes for the 2060s assumes both the bias in Mk3.5 surface fluxes and the daily variability in the surface fluxes do not change between 2060s and 1990s.

The terms used in the 2060s forcing are:

$$\text{forcing (2060s)} = \text{forcing (1990s)} + \text{Mk3.5 projected changes (2060s -1990s)} \quad (2)$$

The initial condition for the OFAM downscaling run for the 2060s is created by adding projected changes in December between the two decades in Mk3.5 ocean fields (temperature, salinity, and velocity), interpolated to OFAM grid, to the initial condition used in the CTRL run. This experiment is denoted “FUTR” hereafter. No further information from Mk3.5 ocean state is used in this experiment.

To deal with the mismatch near the ocean/land boundaries in the low-resolution Mk3.5 fields and high-resolution OFAM fields, the land values in Mk3.5 are masked out first, then interpolated (and extrapolated near the land boundary) to the high-resolution OFAM grid for both initial condition and forcing fields. This approach is based on the understanding that local winds near the coast are unimportant compared to large-scale wind field in the Pacific in driving the EAC and LC (Ridgway and Dunn, 2003; Feng et al., 2003).

A summary of the downscaling experiments is provided in Table 1. Note both experiments are run with repeat-year forcing. While the CTRL run is 26-year long, the FUTR run is 16-year long. It is known that tropical and subtropical thermocline equilibrates to external forcing on a 10-20 year timescale (Sarmiento, 1983; Cox and Bryan, 1983). However, computational constraint precludes long runs. We tested for the stability of our simulations and found little drift in the upper ocean after 5 years.

In the following analyses, the last 10 years of simulation for each experiment are used to compute annual and seasonal fields.

3. Results

a. Overview

In presenting our results, we focus on the similarities and differences between climate projections from the MK3.5 coupled climate model and ocean downscaling simulations from OFAM. Overall, the Mk3.5 simulates relatively broad currents with little fine detail, due to its coarse resolution (Figure 2a). Mk3.5 time-mean circulation does not show a well-defined Leeuwin Current – no coherent flow down the Western Australia coast and around Cape Leeuwin - only weak broad southward flow in the South Indian Ocean (Figure 2a). In comparison, the time-mean circulation in the 1990s simulated by OFAM (Figure 2b) shows much stronger flows with finer structure. In particular, the Leeuwin Current can be seen clearly in OFAM starting from the Northwest Cape (around 22°S), going down the Western Australia coast, turning around the Cape Leeuwin at about 35°S, and extending all the way to the Tasmania Coast to form the South Australian Current (between the eastern Great Australian Bight and western Bass Strait) and the Zeehan Current (off western Tasmania). These features of the LC are consistent with observations (Ridgway and Condie, 2004).

The difference in the upper ocean circulation of the two models is even more pronounced in monthly snapshots (Figure 2c, d). In Mk3.5, the circulation is still smooth (Figure 2c) and shows little difference to the time-mean circulation (Figure 2a). By contrast, a snapshot of OFAM's circulation is dominated by eddies and jets (Figure 2d), features that are averaged out in the time-mean circulation (Figure 2b).

The EAC is a western boundary current that flows poleward from the southern Coral Sea to the coast of northern New South Wales, then separates from the coast between 32-34°S to form the eastward flowing current along the Tasman Front and the EAC Extension, a southward flowing eddy field (Ridgway and Dunn, 2003). Mk3.5 simulates the EAC as a western boundary current; however, the current magnitude of the EAC is too weak (Figure 2a, c). Note that the current speed showing in Figure 2 is depth-averaged over the top 200m. This depth-averaged current speed is proportional to volume transport in the top 200m, so it can be used as a proxy as volume transport. Hereafter, we will use the word circulation and transport interchangeably when referring to depth-averaged current speed. Note the banded structure in the EAC extension from OFAM (Figure 2c) is a consequence of long-term averaging of warm core eddies moving down the coast, which produce a pattern of southward flow near the coast (first band of high flow) and northward flow off-shore (second band of high flow) separated from the EAC (Figure 2d).

To aid in the comparison of Mk3.5 and OFAM simulations, we focus on three upper ocean regions identified in Figure 2a and 2c: the magenta line shows the section to compute Indonesian Throughflow transport, the blue box for the Leeuwin Current, and the Red box for the EAC.

b. The Indonesian Throughflow (ITF)

In OFAM there are three exit straits of the Indonesian throughflow (ITF): the straits of Lombok, Ombai, and Timor, while MK3.5 only resolves outflow through Timor Passage, which is too wide (Fig. 3a). Thus, the strength of the ITF in OFAM is estimated as the combined transport through the three exit straits, following Schiller et al. (2008). The ITF strength in Mk3.5 is approximated by the net zonal transport across a section at 115°E (Fig. 3b), similar to the approach by England and Huang (2005), where they calculated the ITF transport in an ocean reanalysis product. The MK3.5 time-mean

zonal velocity along 115°E is mostly westward down to 1200m depth, similar to but weaker than the OFAM zonal velocity along 115°E (Fig. 3d). OFAM-simulated zonal velocity at Timor Strait at 124.5°E is shown in Fig. 3c, which has predominantly westward flow with greatest flow in the upper 200 m.

Both Mk3.5 and OFAM simulate a reduction in the ITF transport between the 2060s and 1990s (Table 2). In Mk3.5, the ITF transport decreases from 14.5 Sv in 1990s to 13.0 Sv in the 2060s (Table 2). In comparison, the downscaled ITF transport declines by about 20%, from 9.6 Sv in the 1990s (CTRL) to 7.7 Sv in the 2060s (FUTR). The CTRL estimate of 9.6 ± 2.1 Sv (standard deviation of the annual transport) is consistent with the estimate of 9.7 ± 4.4 Sv (standard deviation of the daily transport) from an ocean reanalysis, the Bluelink Ocean ReAnalysis (BRAN), from October 1992 to June 2006 (Schiller et al., 2008). However, these values are lower than a recent calculation of 15 Sv from the 3-year INSTANT field observation from January 2003 to December 2006, but agree with other pre-INSTANT observations reported in the literature (e.g., Spintall et al., 2009; Gordon et al., 2010). The differences among the pre-INSTANT observations, INSTANT observations, Mk3.5, and OFAM values could be due to many factors, such as interannual and decadal variability, different large-scale wind forcings in Mk3.5 and OFAM, model resolution, model parameterizations, etc. However, it is beyond the scope of this paper to address this issue in more detail here.

The seasonal cycle of ITF transport from Mk3.5 and OFAM, as well as individual transport from each outflow strait in OFAM are shown in Figure 4. OFAM exhibits a more pronounced seasonal cycle than Mk3.5. There is also a suggestion from OFAM that there is some seasonality in the projected change, with the greatest decline in the months of January-April.

c. The Leeuwin Current (LC)

On the west coast, the Leeuwin Current is the prominent ocean current. However, probably due to its coarse resolution, Mk3.5 lacks a clearly defined boundary current north of 30°S, and has only a weak broad southward flow in the Southern Indian Ocean next to the Western Australia coast (Fig. 5). In January, there is no southward flowing boundary current in Mk3.5; flow is instead slightly northwards. The differences in Mk3.5 upper ocean circulation off the coast of Western Australia between the 2060s and 1990s show little changes in summer (Fig. 5c), but a clear weakening in the winter (Fig. 5f).

By contrast, OFAM shows a well-defined LC both in the austral summer and winter, with a much stronger current in the winter (Fig. 6), consistent with observed seasonality (Feng et al., 2003). A zoomed view of the LC extending from the coast to 110E is shown in Fig. 7. The LC is much weaker in austral winter in the 2060s than in the 1990s (Fig. 7f), while the change in the austral summer, when the current is much weaker, is small (Fig. 7c).

To provide a more quantitative analysis, we examine the LC strength at in a latitude band between 32°S and 34°S. Within this latitude band, a well defined boundary current exists throughout the year in both models, and there exists observational estimate of LC transport at 32°S (Feng et al., 2003). In Mk3.5, we choose the longitude of 108°E as the western extent to estimate the Mk3.5 LC transport from southward flow in the top 200m. The Mk3.5 LC transport (averaged over 32°S and 34°S) is 1.7 Sv in the 1990s and 1.3 Sv in the 2060s, a reduction of about 20%. In OFAM, LC transport is calculated from southward flow in the top 200m from the coast to 114°E between 32°S and 34°S. The OFAM annual mean LC transport is 2.2 Sv in the 2060s from FUTR, about 15% weaker than 2.7 Sv in the 1990s from CTRL (Table 2).

Both models show that the LC is stronger in the winter and weaker in the summer (Figure 8), with the highest transport in June, consistent with observed seasonality (e.g., Feng et al., 2003). The biggest projected reduction in the LC transport in OFAM is during the season when the mean flow is at its maximum from April to July, while Mk3.5 has the greatest reduction from June to October.

d. The East Australian Current (EAC)

With climate change, Mk3.5 simulates a strengthening in the EAC extension region, which is in general agreement with most other CMIP3 climate models (Sen Gupta et al, 2009). However, Mk3.5 simulates a slight weakening in the core of the EAC between 26°S and 32°S (Fig. 9). By contrast, OFAM simulates a vigorously strengthening EAC system; both the core of the EAC and the EAC extension strengthen with climate change. The strengthening can be seen along the EAC main path between 24°S and 33°S, where it separates from the coast, and also further south in the EAC extension region (Fig. 9).

To quantify the difference in EAC transport between Mk3.5 and OFAM, we compute the EAC transport as depth-integrated southward flow from 148°E to 157°E in the top 600m as a function of latitude (Fig. 10). The Mk3.5 EAC transport changes with latitude smoothly and gradually, and peaks at about 29°S in both periods of the 1990s and 2060s. The EAC transport from OFAM in both periods changes more drastically with latitude and peaks around 32°S, but remains nearly constant from about 35°S to 42°S. Both the EAC core and extension strengthen in OFAM, but there is slight decrease in the recirculation region around 33°S to 36°S. Note that the absolute value of the EAC transport will depend on the choice of longitudinal extent and the vertical extent chosen. To obtain representative values in Mk3.5 and OFAM for the core and extension of EAC transport, we computed the transport over two latitude bands: 28°S to 32°S for the EAC core, and 38°S to 42°S for the EAC extension. Between the 1990s and 2060s, the OFAM EAC transport increases about 12% (from 34 Sv to 38 Sv) in

its core region, and 35% (from 18 to 25 Sv) in its extension, while Mk3.5 EAC transport decreases about 6% (from 19 to 18 Sv) in the core, and increases about 40% (from 6 to 9 Sv) in its extension (Table 2).

With climate change, Mk3.5 simulates a slight weakening in EAC transport along its main path (north of 32°S) between the two time periods, but OFAM simulates a strengthening in the EAC transport both north and south of the peak value at 32°S, with the development of a second maximum at 39°S as the EAC extension entrains more off-shore water into its flow.

4. Summary and discussion

The present study seeks to quantify the response of the Australian boundary currents, the EAC and LC in particular, to climate change using ocean dynamical downscaling. The approach uses bias-corrected surface fluxes from climate change projections under the SRES A1B scenario by the CSIRO Mk3.5 climate model to force an eddy-resolving ocean model in the Australian region, the OFAM model. The EAC and LC are generally poorly represented by coarse-resolution climate models. However, they are primarily driven by large-scale wind fields, which are resolved by climate models. It is therefore feasible to simulate the changes in these boundary currents in a future climate by forcing a high-resolution ocean model with output from climate model projections. To this end we investigate the impact of climate change on the LC, EAC and the ITF by examining the difference in these currents between the 2060s and 1990s.

The 1990s climate is downscaled by driving OFAM with the air-sea fluxes from the ERA40 Reanalysis. OFAM is able to reproduce key features of the EAC and LC in the 1990s, such as their spatial structure, seasonality, and volume transports, which are poorly represented in the Mk3.5 model.

To produce the downscaled climate in the 2060s, we apply a bias correction technique, whereby the difference between the Mk3.5 2060s and 1990s air-sea fluxes (momentum, heat, and fresh water fluxes) are added to the ERA40 forcing used in the control experiment.

While it is possible to assess the response of ocean boundary currents to climate change from coupled climate models, important features such as spatial structure are missing in climate models due to the resolution. The downscaling captures finer-scale features and realistic volume transports of the boundary currents, thus provides additional information on the impact of climate change.

The downscaling projects a 15% decrease in the LC transport (between 32°S and 34°S) between the 1990s and 2060s. The weakening of the LC in the 2060s can be attributed to changes in the large-scale wind forcing in the equatorial Pacific simulated by Mk3.5. A weakening of the tropical atmospheric circulation in response to global warming is a robust feature across an ensemble of 22 IPCC AR4/CMIP3 climate models, including Mk3.5 (Vecchi and Soden 2007). Mk3.5 zonal windstress in the equatorial Pacific displays a weakening trend from 1850s to 2100 under SRES A1B scenario (Fig. 12), consistent with the sign of change observed in the 20th century (Vecchi et al. 2006, Fig. 4). The weakened zonal windstress in the equatorial Pacific leads to weakened ITF and LC in both Mk3.5 and the downscaling, as the LC is primarily forced by the meridional pressure gradient associated with the ITF (Godfrey and Ridgway, 1985; McCreary 1986). The projected weakening of the ITF and LC in the 2060s from the Mk3.5 and ocean downscaling are similar, but Mk3.5 does not resolve the coastal waveguide and has an unrealistically wide LC that is non-existent in the summer. In the downscaling projection, the largest reduction in the LC occurs in the austral winter, when the current is also the strongest. The weakening trend of the ITF and LC into the future is consistent with observations from the past several decades (Feng et al., 2004; Wainwright et al., 2008), although a

recent study suggests the trend over the past 15 years has reversed sign with increasing transport, likely a result of decadal variability (Feng et al., 2010; Feng et al., 2011).

The EAC strengthens in the 2060s due to the strengthening and southward shift of basin-wide wind stress curl in the South Pacific simulated by Mk3.5, which is also a robust feature in the majority of CMIP3 climate models (Cai 2005; Sen Gupta et al., 2009). This strengthening is consistent with observations and modeling results over past decades (e.g., Cai 2006; Ridgway et al. 2007, 2008; Hill et al. 2008), as a result of increased wind stress curl in the South Pacific, as explained by Sverdrup dynamics (e.g., Roemmich et al., 2007; Hill et al. 2008). However, in Mk3.5, the EAC core does not strengthen and only the EAC extension strengthens. The downscaling projects a consistent strengthening of both the EAC core and EAC extension, about 10% increase in the EAC core and 35% increase in the EAC extension.

To assess if the difference between the two decades of 2060s and 1990s is representative of long term trends, we compute the Mk3.5 EAC core transport (averaged over 28-32°S) and EAC extension transport (averaged over 38-42°S) from 1980 to 2100 (Fig. 12). The change between the two decades used in this study is consistent with the Mk3.5 long-term trend, which shows that the EAC core slightly weakens but the EAC extension strengthens. The changes in ITF and LC between 1990s and 2060s in Mk3.5 are also consistent with the long-term trend in Mk3.5 simulations (not shown).

The present study focuses on hydrodynamic changes in the boundary currents, which provides an important first step for investigating the ecological impacts of climate change. The differences between the ocean downscaling and Mk3.5 in the projected changes in the 2060s for both the LC and EAC will have important implications for marine biology, connectivity, and water mass formation (e.g., Poloczanska et al., 2008, 2009; Diteze et al., 2009; Stock et al., 2011).

One caveat of marine downscaling is that there is no feedback of the ocean state to the atmosphere. The use of an ocean-only model for downscaling neglects the potential feedback a change in the ocean state may have on the exchange of heat, water and momentum between the atmosphere and ocean. In this study, the ocean climate change projection is based on the difference of climate projections between two decades from one climate model and one emission scenario. To assess the robustness of climate projection, different projections from different climate models under various scenarios could be used to force the ocean downscaling model. Further, the use of the climate anomaly approach (Eq. 1) to reduce climate model biases assumes we could treat climate change independently of the ocean state of the climate model. The consequence of this assumption on the downscaled projections needs to be investigated. It is conceivable that downscaled atmospheric forcing could also alter ocean downscaling (e.g. Langlais et al., 2009) and should be investigated.

Finally, as in all climate model projections, the assessment of projections is limited by lack of future data. An important next step is to assess the robustness of projections from ocean downscaling against past trends and to investigate the limitations discussed above on the climate projections.

Acknowledgments.

The OFAM simulations have been carried out at the Australian National Computing Infrastructure (NCI) supercomputing facility. Initial test runs were performed at the iVEC supercomputing facility in Western Australia. The FERRET program was used for analysis and graphics (<http://ferret.pmel.noaa.gov/Ferret/>). The authors thank Graham Symonds, Stuart Godfrey, Jay

McCreary, Tony Hirst, Wenju Cai, and Evan Weller for helpful discussions; Russ Fiedler for OFAM tips; Chris Hines, Stephen Leak, Stephen Phipps, Margaret Khan, and David Singleton for supercomputing help; Gareth Williams for help archive model output data at the iVEC; Alf Uhlherr, Robert Bell, Ben Evans, Paul Tildesley, and Robert Mollard for help with supercomputing resources; and FERRET user community for useful tips. Constructive and insightful comments from two anonymous reviewers helped improve the paper significantly. This work is supported by the Western Australian Marine Science Institution (WAMSI).

REFERENCES

- Ådlandsvik, B., and M. Bentsen, 2007: Downscaling a twentieth century global climate simulation to the North Sea. *Ocean Dyn.*, **57**, 453-466, DOI: 10.1007/s10236-007-0125-2.
- Ådlandsvik, B., 2008: Marine downscaling of a future climate scenario for the North Sea. *Tellus*, **60**(3): 451-458.
- Auad, G., A. J. Miller and E. Di Lorenzo, 2006: Long term forecast of oceanic conditions off California and their biological implications. *J. Geophys. Res. Oceans*, 111, C09008, DOI:10.1029/2005JC003219.
- Booth, D.J., Figueira, W.F., Gregson, M.A., Brown, L. and Beretta, G., 2007: Occurrence of tropical fishes in temperate southeastern Australia: role of the East Australian Current. *Estuarine Coastal and Shelf Science*, 72, 102-114. doi:10.1016/j.ecss.2006.10.003.
- Cai, W., G. Shi, T. Cowan, D. Bi, and J. Ribbe: The response of the Southern Annular Mode, the East Australian Current, and the southern mid-latitude ocean circulation to global warming. *Geophys. Res. Lett.*, **32**, L23706, doi:10.1029/2005GL024701.
- Cai, W., 2006: Antarctic ozone depletion causes an intensification of the Southern Ocean super-gyre circulation. *Geophys. Res. Lett.*, **33**, L03712, doi:10.1029/2005GL024911.
- Caldwell, P., H.-N. Chin, D. C. Bader, and G. Bala, 2009: Evaluation of a WRF dynamical downscaling simulation over California. *Climatic Change*, **95**(3), 499-521.
- Chiswell, S.M., Toole, J., Church, J., 1997: Transports across the Tasman Sea from WOCE repeat sections: the East Australian Current 1990-94. *N. Z. J. Mar. Freshwater Res.*, **31**, 469-475.
- Cox, M.D. and K. Bryan, 1984: A numerical model of the ventilated thermocline. *J. Phys. Oceanogr.*, **14**, 674-687.
- Dietze, H., R. Matear, and T. Moore, 2009: Nutrient supply to anticyclonic meso-scale eddies off western Australia estimated with artificial tracers released in a circulation model. *Deep Sea Res.*, **56**, 1440-1448.
- Emanuel, K., 2006: Climate and Tropical Cyclone Activity: A New Model Downscaling Approach. *J. Climate*, **19**, 4797-4802.
- Emanuel, K., R. Sundararajan, and J. Williams, 2008: Hurricanes and Global Warming: Results from Downscaling IPCC AR4 Simulations." *Bull. Amer. Meteor. Soc.*, **89**(3), 347-367.
- England, M.H. and F. Huang, 2005: On the interannual variability of the Indonesian Throughflow and its linkage with ENSO. *J. Climate*, **18**, 1435-1444.
- Feng, M., G. Meyers, A. Pearce, and S. Wijffels, 2003: Annual and interannual variations of the Leeuwin Current at 32°S, *J. Geophys. Res.*, **108**(C11), 3355, doi:10.1029/2002JC001763.

- Feng, M., Y. Li, and G. Meyers, 2004: Multidecadal variations of Fremantlesea level: Footprint of climate variability in the tropical Pacific. *Geophys. Res. Lett.*, **31**, L16302, doi:10.1029/2004GL019947.
- Feng, M., M. J. McPhaden, and T. Lee, 2010: Decadal variability of the Pacific subtropical cells and their influence on the southeast Indian Ocean. *Geophys. Res. Lett.*, **37**, L09606, doi:10.1029/2010GL042796.
- Feng, M., C. Böning, A. Biastoch, E. Behrens, E. Weller, and Y. Masumoto, 2011: The reversal of the multi-decadal trends of the equatorial Pacific easterly winds, and the Indonesian Throughflow and Leeuwin Current transports. *Geophys. Res. Lett.*, **38**, L11604, doi:10.1029/2011GL047291.
- Godfrey, J.S. and Ridgway, K.R., 1985: The large-scale environment of the poleward flowing Leeuwin Current, Western Australia: Longshore steric height gradients, wind stresses, and geostrophic flow. *J. Phys. Oceanogr.*, **15**, 481-495.
- Gordon, A. L J. Sprintall, H.M. Van Aken, D. Susanto, S. Wijffels, R. Molcard, A. Ffield, W. Pranowo and S. Wirasantos, 2010: The Indonesian throughflow during 2004-2006 as observed by the INSTANT program. *Dyn. Atmos. Oceans*, **50**(2), 115-128.
- Gordon, H.B., Rotstayn, L.D., McGregor, J.L., Dix, M.R., Kowalczyk, E.A., O'Farrell, S.P., Waterman, L.J., Hirst, A.C., Wilson, S.G., Collier, M.A., Watterson, I.G., T, I.E., 2002: The CSIRO Mk3 Climate System Model. CSIRO Techreport, 130.
- Griffies, S., M. J. Harrison, R. C. Pacanowski, and A. Rosati, 2004: A Technical Guide to MOM4, GFDL Ocean Group Technical Report No. 5, Princeton, NJ. NOAA/Geophysical Fluid Dynamics Laboratory, 342 pp.
- Griffies, S. M., Gnanadesikan A, Dixon KW, Dunne J, Gerdes A, Harrison MJ, Rosati A, Russel J, Samuels BL, Spelman MJ, Winton M, Zhang R, 2005: Formulation of an ocean model for global climate simulations. *Ocean Sci.*, **1**, 45–79.
- Hill, K. L., S. R. Rintoul, R. Coleman, and K. R. Ridgway, 2008: Wind forced low frequency variability of the East Australia Current. *Geophys. Res. Lett.*, **35**(8).

- Hill, K. L., S. R. Rintoul, K. R. Ridgway, and P. R. Oke, 2011: Decadal changes in the South Pacific western boundary current system revealed in observations and ocean state estimates, *J. Geophys. Res.*, **116**, C01009, doi:10.1029/2009JC005926.
- Langlais, C., B. Barnier, et al., 2009: Evaluation of a dynamically downscaled atmospheric reanalyse in the prospect of forcing long term simulations of the ocean circulation in the Gulf of Lions. *Ocean Modelling*, **30**(4), 270-286.
- Lenanton, R. C., N. Caputi, M. Kangas, M. Craine, 2009: The ongoing influence of the Leeuwin Current on economically important fish and invertebrates off temperate Western Australia - has it changed? *J. Royal Soc. of W. Australia*, **92**(2): 111-127.
- Mata, M., M. Tomczak, S. Wijffels, and J. Church, 2000: East Australian Current volume transports at 30°S: Estimates from the World Ocean Circulation Experiment hydrographic sections PR11/P6 and the PCM3 current meter array. *J. Geophys. Res.*, **105**(C12), 28509-28526.
- McCreary, J., S. R. Shetye, and P. K. Kundu, 1986: Thermohaline forcing of eastern boundary currents: With application to the circulation off the west coast of Australia. *J. Mar. Res.*, **44**, 71-92.
- H. E. M. Meier, 2006: Baltic Sea climate in the late twenty-first century: a dynamical downscaling approach using two global models and two emission scenarios. *Clim. Dyn.*, **27** (1), 39-68.
- Oke, P. R., A. Schiller, G. A. Griffin, G. B. Brassington, 2005: Ensemble data assimilation for an eddy-resolving ocean model. *Quarterly Journal of the Royal Meteorological Society*, **131**, 3301-3311.
- Oke, P.R., Brassington, G.B., Griffin, D.A., Schiller, A., 2008. The Bluelink ocean data assimilation system (BODAS). *Ocean Modelling*, **21**, 46–70.
- Poloczanska, E. S., R. C. Babcock, A. Butler, A. J. Hobday, O. Hoegh-Guldberg, T. J., Kunz, R. Matear, D. A. Milton, T. A. Okey, A. J. Richardson, 2007: Climate change and Australian marine life. *Oceanography and Marine Biology: an Annual Review*, **45**, 407-478.
- Poloczanska, E. S., S. J. Hawkins, A. J. Southward, M.T., Burrows, 2008. Modelling the response of populations of competing species to climate change. *Ecology*, **89**, 3138-49.

- Reichler, T. and J. Kim, 2008: How Well Do Coupled Models Simulate Today's Climate? *Bull. Amer. Meteor. Soc.*, **89**, 303-311.
- Ridgway, K. R., 2007: Long-term trend and decadal variability of the southward penetration of the East Australian Current, *Geophys. Res. Lett.*, **34**, L13613, doi:10.1029/2007GL030393.
- Ridgway, K. R. and S. A. Condie, 2004: The 5500-km-long boundary flow off western and southern Australia. *J. Geophys. Res.*, **109**(C4), C04017.
- Ridgway, K. R., and J. R. Dunn, 2003: Mesoscale structure of the mean East Australian Current System and its relationship with topography. *Progress in Oceanography*, **56**(2): 189-222.
- Ridgway, K.R., Godfrey, J.S., 1997: Seasonal cycle of the East Australian Current. *J. Geophys. Res.*, **102**, 22,921–22,936.
- Ridgway, K. R., R. C. Coleman, R. J. Bailey, and P. Sutton, 2008: Decadal variability of East Australian Current transport inferred from repeated high-density XBT transects, a CTD survey and satellite altimetry, *J. Geophys. Res.*, **113**, C08039, doi:10.1029/2007JC004664.
- Reichler, T. and J. Kim, 2008: How Well Do Coupled Models Simulate Today's Climate? *Bull. Amer. Meteor. Soc.*, **89**, 303-311.
- Roemmich, D., J. Gilson, R. Davis, P. Sutton, S. Wijffels, S. Riser, 2007: Decadal Spinup of the South Pacific Subtropical Gyre. *J. Phys. Oceanogr.*, **37**, 162–173.
- Sarmiento, J. L., 1983: A tritium box model of the North Atlantic thermocline, *J. Phys. Oceanogr.*, **13**, 1269-1274.
- Schiller, A., P. R. Oke, G. Brassington, M. Entel, R. Fiedler, D.A. Griffin and J.V. Mansbridge, 2008: Eddy-resolving ocean circulation in the Asian-Australian region inferred from an ocean reanalysis effort. *Progress in Oceanography*, **76**(3): 334-365.
- Sen Gupta, A., A. Santoso, A. S. Taschetto, C. C. Ummenhofer, J. Trevena, M. H. England, 2009: Projected Changes to the Southern Hemisphere Ocean and Sea Ice in the IPCC AR4 Climate Models. *J. Climate*, **22**, 3047–3078. DOI: 10.1175/2008JCLI2827.1.

- Solomon, S., 2007: Climate change 2007: the physical science basis : contribution of Working Group I to the Fourth Assessment Report of the Intergovernmental Panel on Climate Change.
- Sprintall, J., S. E. Wijffels, R. Molcard, and I. Jaya, 2009: Direct estimates of the Indonesian Throughflow entering the Indian Ocean: 2004-2006. *J. Geophys. Res.*, **114**, C07001, doi:10.1029/2008JC005257.
- Stock, C.A., Alexander, M.A., Bond, N.A., Brander, K., Cheung, W.W.L., Curchitser, E.N., Delworth, T.L., Dunne, J.P., Griffies, S.M., Haltuch, M.A., Hare, J.A., Hollowed, A.B., Lehodey, P., Levin, S.A., Link, J.S., Rose, K.A., Rykaczewski, R.R., Sarmiento, J.L., Stouffer, R.J., Schwing, F.B., Vecchi, G.A., Werner, F.E., 2011: On the use of IPCC-class models to assess the impact of climate on living marine resources. *Progress in Oceanography*, **88**, 1-27. doi: 10.1016/j.pocean.2010.09.001.
- Uppala, S. M., KÅllberg, P. W., Simmons, and co-authors, 2005: The ERA-40 re-analysis. *Q. J. Royal Meteor. Soc.*, **131**, 2961–3012. doi: 10.1256/qj.04.176.
- Vecchi, G. A., B. J. Soden, et al., 2006: Weakening of tropical Pacific atmospheric circulation due to anthropogenic forcing. *Nature*, **441**(7089): 73-76.
- Vecchi, G. A., and B. J. Soden, 2007a: Global warming and the weakening of the tropical circulation. *J. Climate*, **20**, 4316–4340.
- Wainwright, L., Meyers, G., Wijffels, S. and Pigot, L., 2008: Change in the Indonesian Throughflow with the climatic shift of 1976/77. *Geophys. Res. Lett.*, **35**: L03604. doi:10.1029/2007GL031911.

	CTRL	FUTR
Ocean initial condition	December 1990s	December 2060s= CTRL initial condition + Mk3.5 (December 2060s-December 1990s)
Forcing	forcing (1990s) = ERA40 monthly climatology + ERA40 daily anomaly (1995) + OFAM spinup flux correction	forcing (2060s) = CTRL forcing + Mk3.5 monthly climatology (2060s-1990s)
Length of simulation	26 years	16 years

Table 1: Summary of surface forcing and initial conditions in different experiments.

	OBS	Mk3.5 (1990s)	OFAM (1990s)	Mk3.5 (2060s)	OFAM (2060s)
ITF	9.7±4.4 (BRAN) 15 Sv (INSTANT)	14.5 ± 0.8	9.6±2.1	13.0 ± 0.9	7.7±2.8
LC (32°S- 34°S)	3.4 Sv at 32°S (Feng et al. 2003)	1.7±0.3	2.7±0.3	1.3 ±0.2	2.2±0.3
EAC core at 28°-32°S	22.1 ± 4.6 Sv at 30°S, coast to 154.4°E (Mata et al., 2000); 27.4 to 36.3 Sv at 28°S, coast to 155.7°E (Ridgway and Godfrey, 1997) ; 22 to 42 Sv at 29°S, coast to 154.8°E (Chiswell et al., 1997) 25 Sv at 29°S, 37 Sv at 33°S (Ridgway and Dunn, 2003)	19.3 ± 1.3	33.7±3.0	18.0 ± 1.3	37.9±2.3
EAC extensionat 38°-42°S	7.1 Sv at 44°S (Ridgway and Godfrey, 1997)	6.4 ± 0.7	18.3 ± 2.2	9.3 ± 1.0	25.0± 2.4

Table 2: Time-mean volume transports of the Indonesian Throughflow (ITF), Leeuwin Current (LC), and the EAC from Mk3.5 and downscaling, and estimates from observations. Note the numbers after ± are standard

deviations of annual volume transports. The LC transport is averaged over a latitude band between 32°S and 34°S, the EAC core transport over 28°S-32°S, and the EAC extensiontransport over 38°S-42°S. BRAN is the Bluelink ReAnalysis from 1992 to 2006 (Oke et al, 2008, Schiller et al. 2008). INSTANT estimate is from a 3-year field program from January 2003 to December 2006 (Spintall et al., 2009; Gordon et al., 2010).

Table of figures:

Figure 1: Zonal wind stress biases in four CMIP3 climate models: (a) GFDL CM2.1; (b) UKMO Hadgem1 (c) CSIRO Mk3.5, and (d) MPI ECHAM5. The bias is calculated over 1981-2000 in N/m^2, using the ERA40 Reanalysis as benchmark.	28
Figure 2: Time-mean circulation in the 1990s from (a) Mk3.5 and (b) OFAM (top), and examples of snapshots (bottom). The colors show the depth-averaged current speed over 0-200m in m/s; color scale is the same in all panels and is shown in (d). Vectors in (a-c) show the direction and magnitude of the depth-averaged current; vector scales are shown. Vectors are omitted in (d) to help visualize the eddies and jets in the flow field. Boxes denote the domain shown in Figure 7, 7 and 8. The magenta lines in (a) and (b) denote the sections used to calculate the ITF transport. The locations of Ombai and Lombok Straits that are used in OFAM for ITF transport calculations are shown in Fig. 2. Shaded gray areas show the land masks in the model.	29
Figure 3: (a) Land masks in Mk3.5 (gray area) and OFAM (black area). Red lines denote the three locations where ITF outflow straits in OFAM used to compute the ITF transport. The blue line is the section at 115°E used to calculate ITF transport for Mk3.5. (b) and (d): 1990s time-mean zonal velocity at 115°E from Mk3.5 and OFAM. (c) 1990s time-mean zonal velocity at Timor Strait from OFAM (124.5°E). Colors in (b-d) are zonal velocity in m/s; eastward is positive (red), westward is negative (blue).	30
Figure 4: Seasonal cycle of ITF transport from Mk3.5 (a) and OFAM (b): 1990s (black), 2060s (red). Mk3.5 transport is from a section at 115E, from 22S to 8.2S, with westward transport positive. Note the scales of the transport on the plots are different.	31
Figure 5: Mk3.5 seasonal circulation off Western Australia from 1990s (a, b), 2060s (c, d), and differences between the two time periods (e, f) for January (left column) and July (right column). Colors show the magnitude of currents (in m/s) depth-averaged over the top 200 m. Vectors show the direction of the depth-averaged current; vector scale shown in (a). Gray shading indicates model land areas; the black lines indicate the actual coastline.	33

Figure 6: OFAM time-mean circulation off Western Australia from CTRL (left) and FUTR (center). Colors show the magnitude of currents (depth-averaged over 0–200 m) in m/s. Vector lengths correspond to velocity magnitude, scale shown in (a). (c, f): Velocity difference in January (c) and July (f) between the two time slices of 2060s and 1990s. The magenta lines indicate 100m and 2000m isobaths. 34

Figure 7: The same as Fig. 6, but for a zoomed view. 35

Figure 8: Seasonal cycle of the Leeuwin Current transport from (a) Mk3.5 and (b) OFAM (b): 1990s (black) and 2060s (red). Southward transport is positive. The Mk3.5 transport is estimated from southward flow averaged over 32°–34°S (0–200m, coast to 108°). LC transport from OFAM is calculated from southward flow (0–200m, coast to 114°E) averaged over 32°–34°S. 36

Figure 9: Time-mean circulation off the east coast of Australia from Mk3.5 (left) and OFAM (right) in the 1990s (top) and 2060s (center) and the differences between the two decades (bottom). Colors show current speed depth-averaged over 0–600 m in cm/s. Vector length represents current speed averaged over 0–600m in cm/s, and the corresponding vector scales are shown in (a-d). Note the scale in (f) is 10 times larger than (c). 37

Figure 10: Annual-mean EAC transport along its path: Mk3.5 (dashed) and OFAM (solid). Red line is 2060s, black 1990s. Transport is calculated as depth-integrated southward flow from 148°E to 157°E, 0–600m. 38

Figure 11: Equatorial Pacific zonal-mean zonal wind stress anomaly (N/m^2) from the Mk3.5 20C3M experiment (1860–2000) and SRES A1B (2001–2100) simulations. The zonal wind-stress anomaly is averaged 120°E–70°W, 5°S–5°N. The cyan curve is the monthly mean, black line the annual mean, and red line the trend. Note that zonal windstress in the equatorial Pacific is westward (negative in this figure), so a positive anomaly indicates a weakening of windstress there. The monthly difference in the wind stress over the global domain from the two time slices (2060s and 1990s) is used to compute a 10-year averaged monthly climatology in the future forcing used in the downscaling experiments. 39

Figure 12: Mk3.5 EAC transport from 1980 to 2100. (a) EAC core transport averaged over 28°–32°S; and (b) EAC extension transport (averaged over 38°S–42°S). Mk3.5 transport is integrated from southward flows 148°E to 160°E, 0–600m. The cyan curve is the monthly mean, blue line the annual mean, and red line the trend. 40

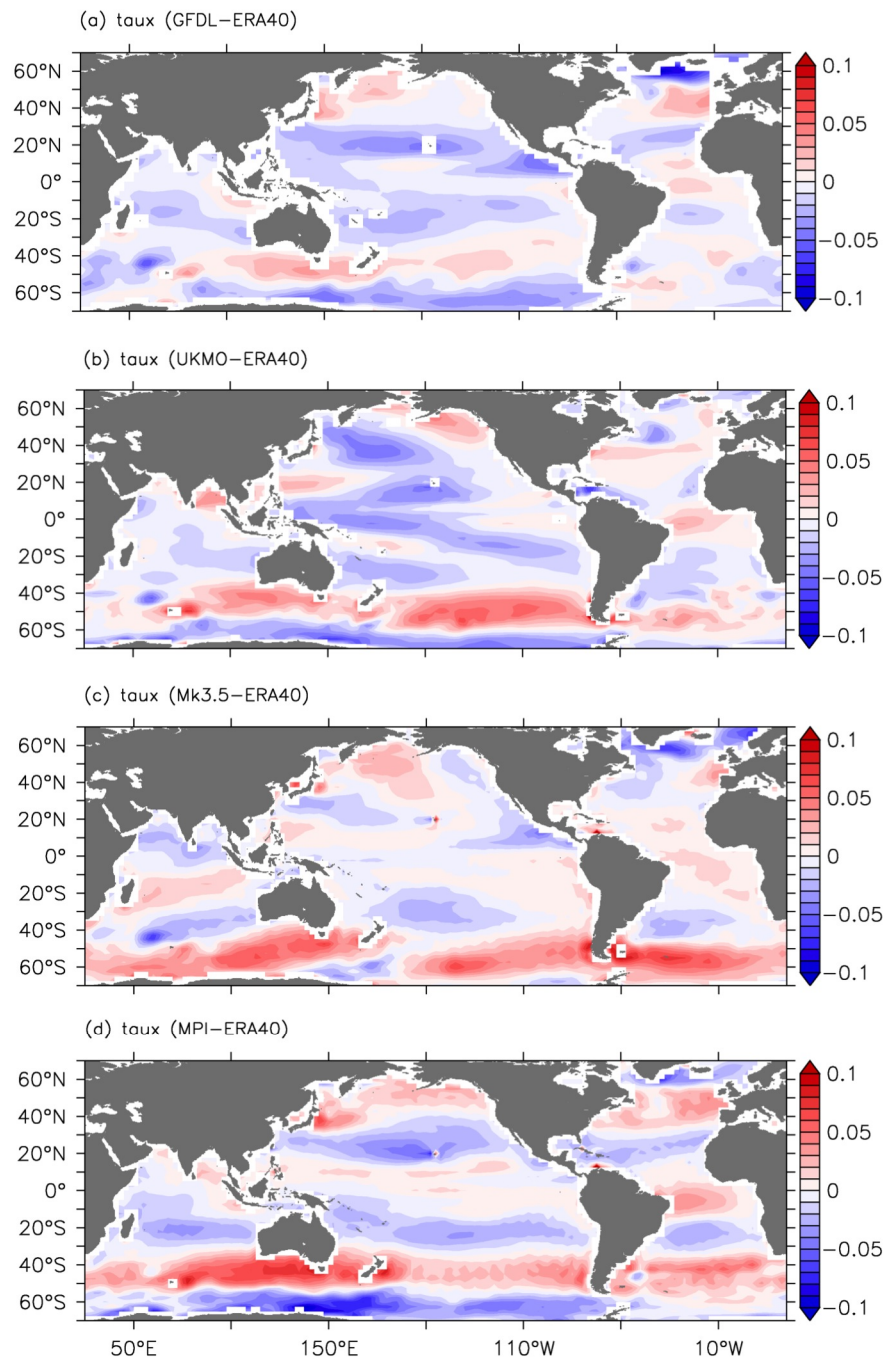


Figure 1: Zonal wind stress biases in four CMIP3 climate models: (a) GFDL CM2.1; (b) UKMO Hadgem1 (c) CSIRO Mk3.5, and (d) MPI ECHAM5. The bias is calculated over 1981-2000 in N/m^2 , using the ERA40 Reanalysis as benchmark.

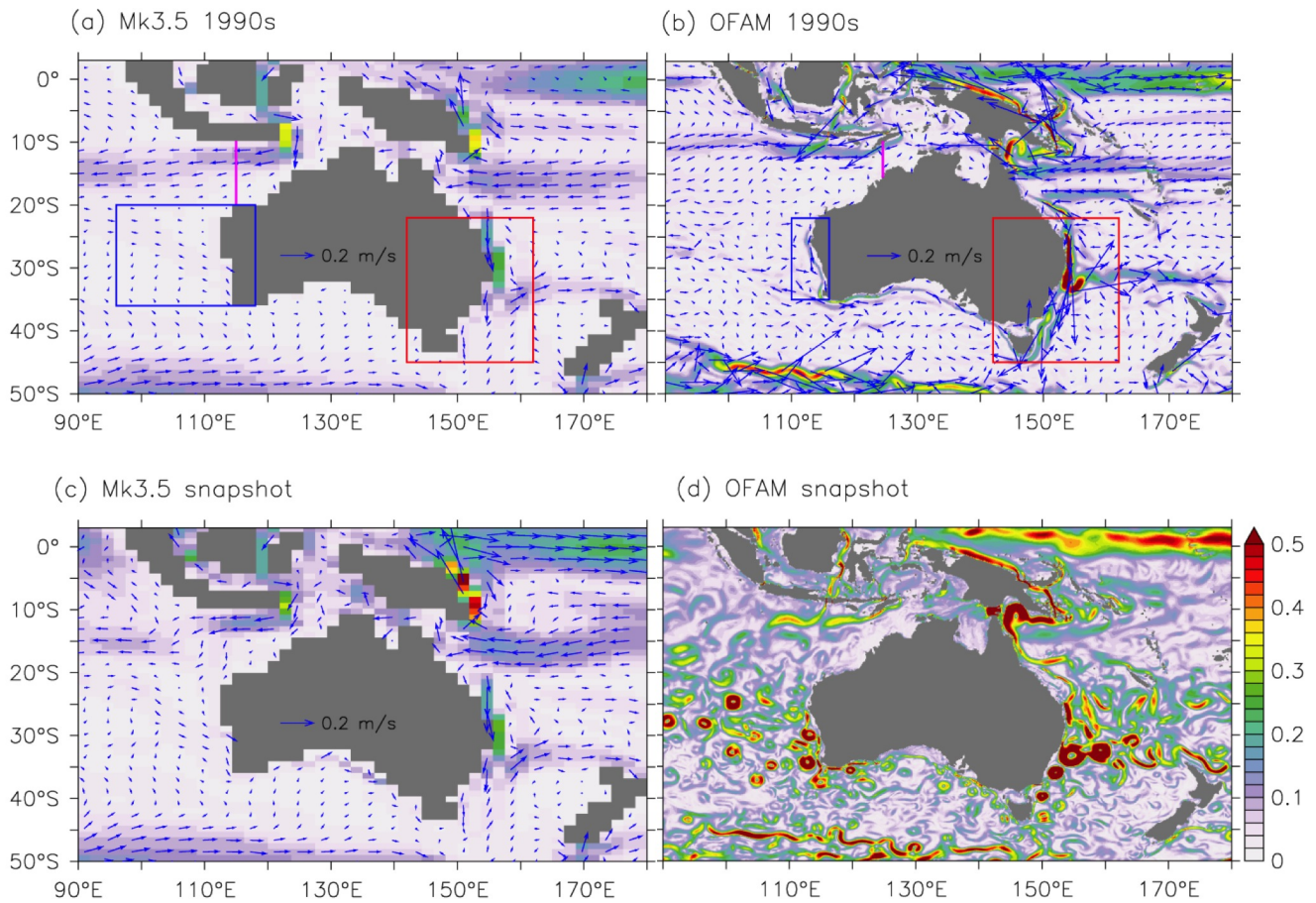


Figure 2: Time-mean circulation in the 1990s from (a) Mk3.5 and (b) OFAM (top), and examples of snapshots (bottom). The colors show the depth-averaged current speed over 0-200m in m/s; color scale is the same in all panels and is shown in (d). Vectors in (a-c) show the direction and magnitude of the depth-averaged current; vector scales are shown. Vectors are omitted in (d) to help visualize the eddies and jets in the flow field. Boxes denote the domain shown in Figure 7, 7 and 8. The magenta lines in (a) and (b) denote the sections used to calculate the ITF transport. The locations of Ombai and Lombok Straits that are used in OFAM for ITF transport calculations are shown in Fig. 2. Shaded gray areas show the land masks in the model.

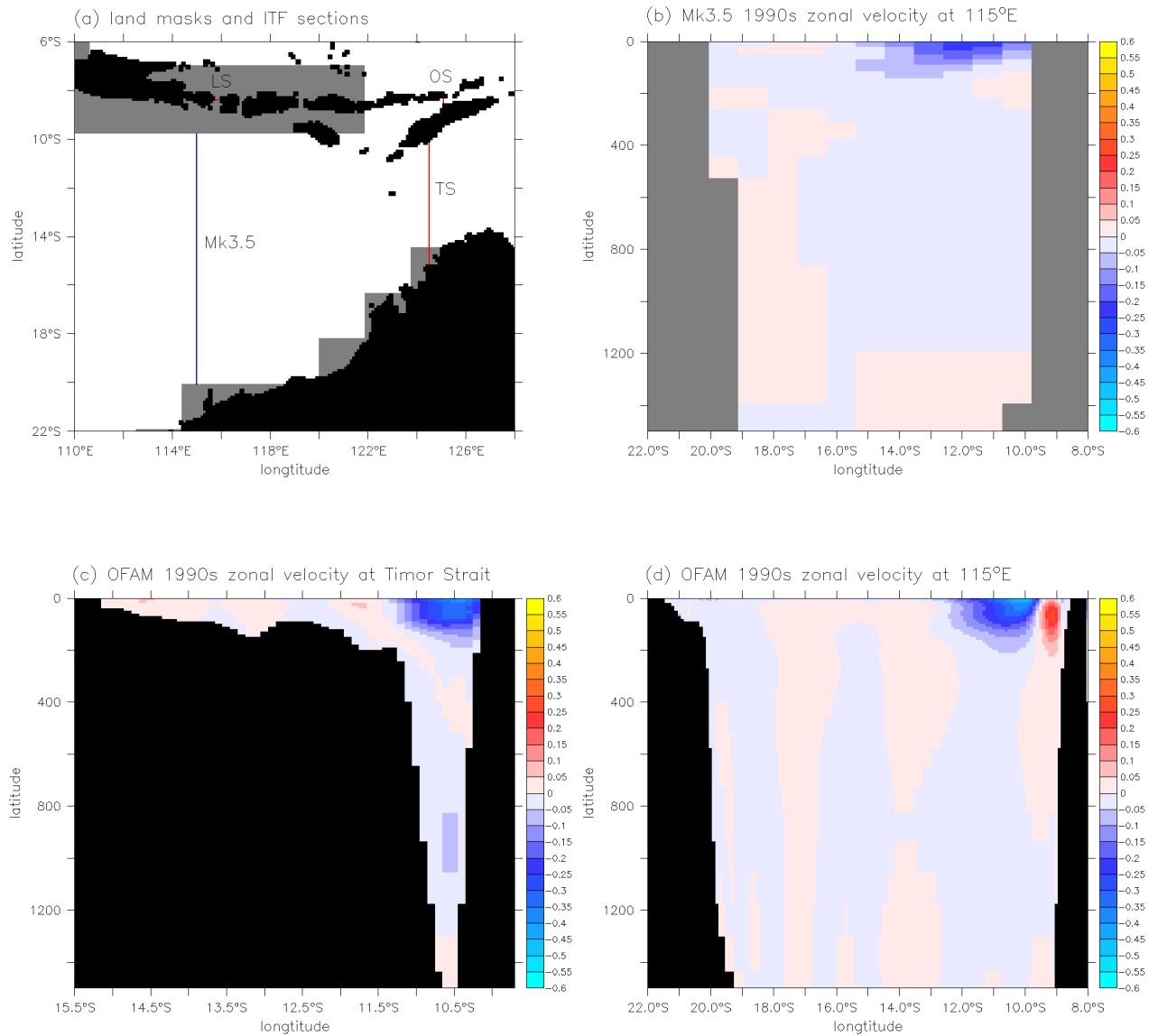


Figure 3: (a) Land masks in Mk3.5 (gray area) and OFAM (black area). Red lines denote the three locations where ITF outflow straits in OFAM used to compute the ITF transport. The blue line is the section at 115°E used to calculate ITF transport for Mk3.5. (b) and (d): 1990s time-mean zonal velocity at 115°E from Mk3.5 and OFAM. (c) 1990s time-mean zonal velocity at Timor Strait from OFAM (124.5°E). Colors in (b-d) are zonal velocity in m/s; eastward is positive (red), westward is negative (blue).

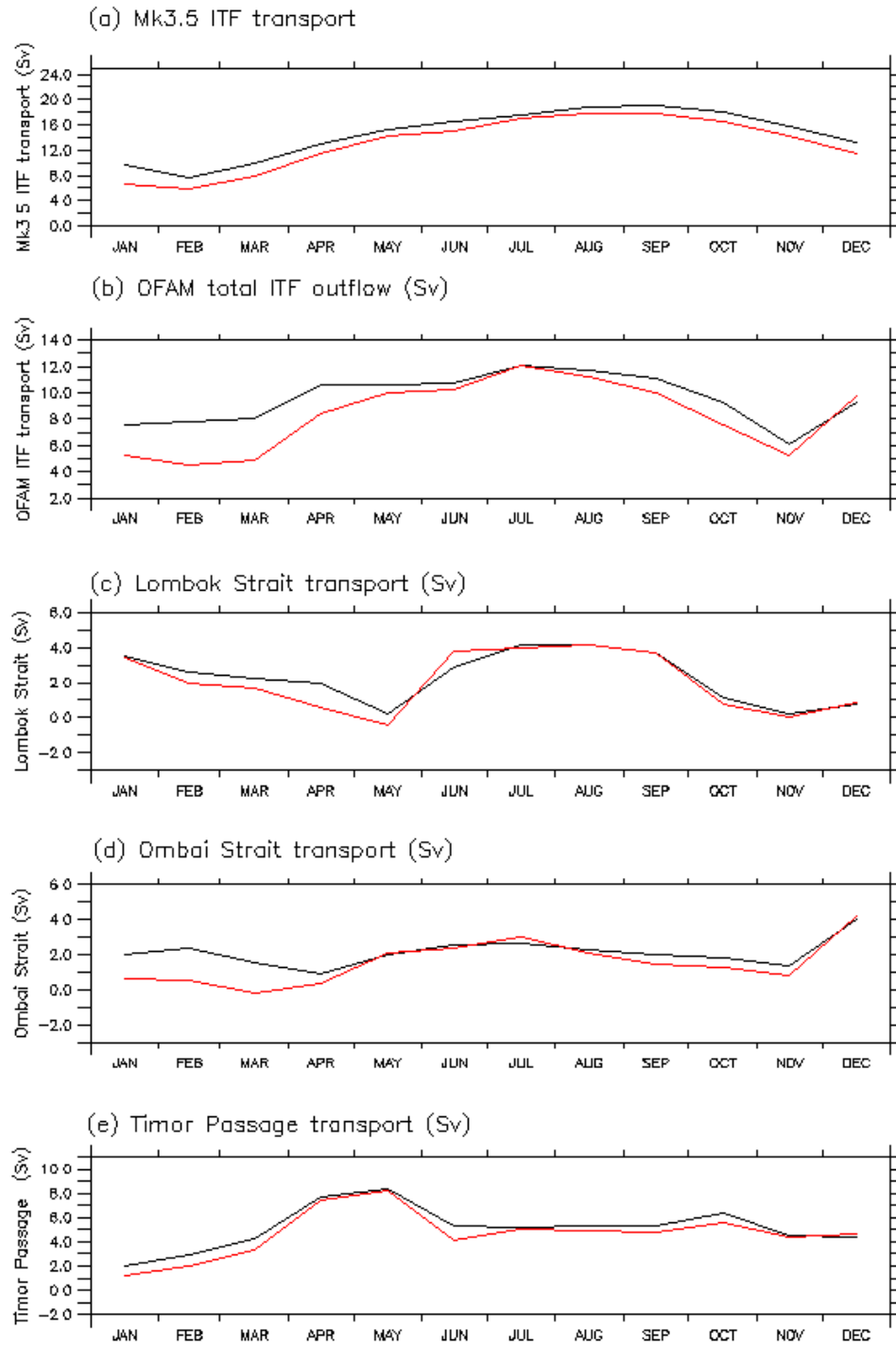


Figure 4: Seasonal cycle of ITF transport from Mk3.5 (a) and OFAM (b): 1990s (black), 2060s (red). Mk3.5 transport is from a section at 115E, from 22S to 8.2S, with westward transport positive. Note the scales of the transport on the plots are different.

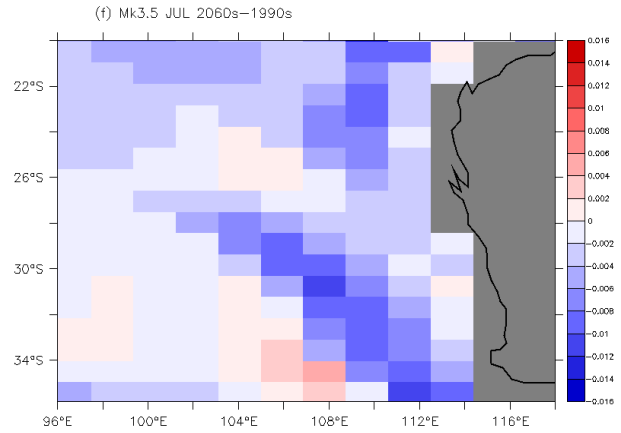
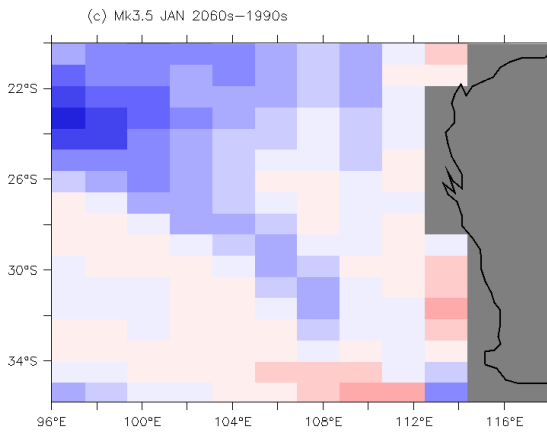
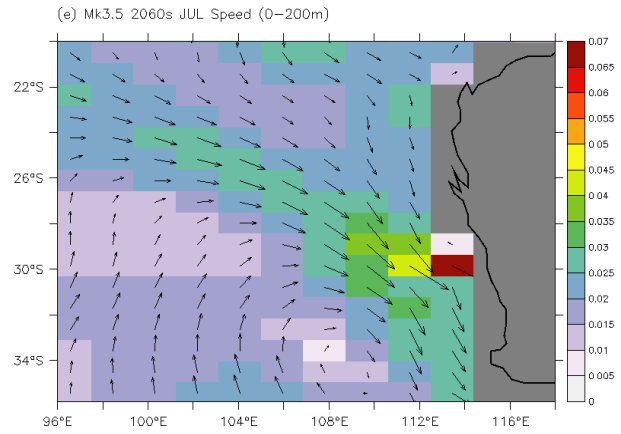
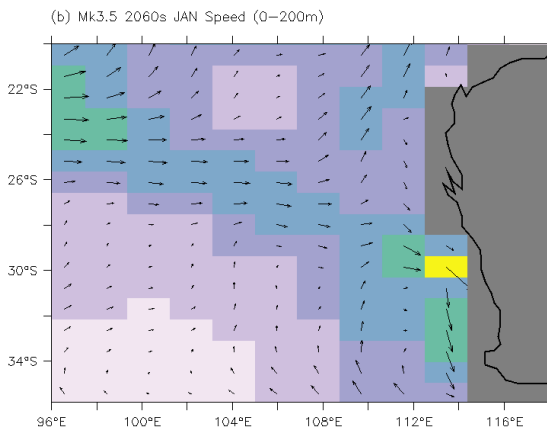
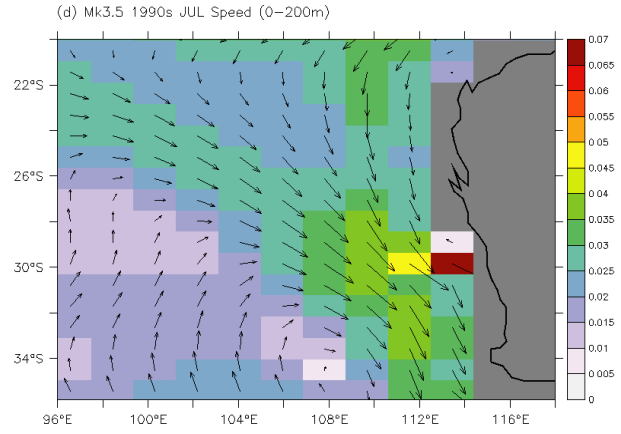
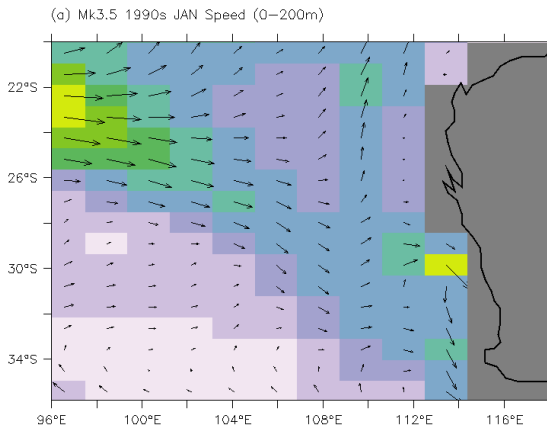


Figure 5: Mk3.5 seasonal circulation off Western Australia from 1990s (a, b), 2060s (c, d), and differences between the two time periods (e, f) for January (left column) and July (right column). Colors show the magnitude of currents (in m/s) depth-averaged over the top 200 m. Vectors show the direction of the depth-averaged current; vector scale shown in (a). Gray shading indicates model land areas; the black lines indicate the actual coastline.

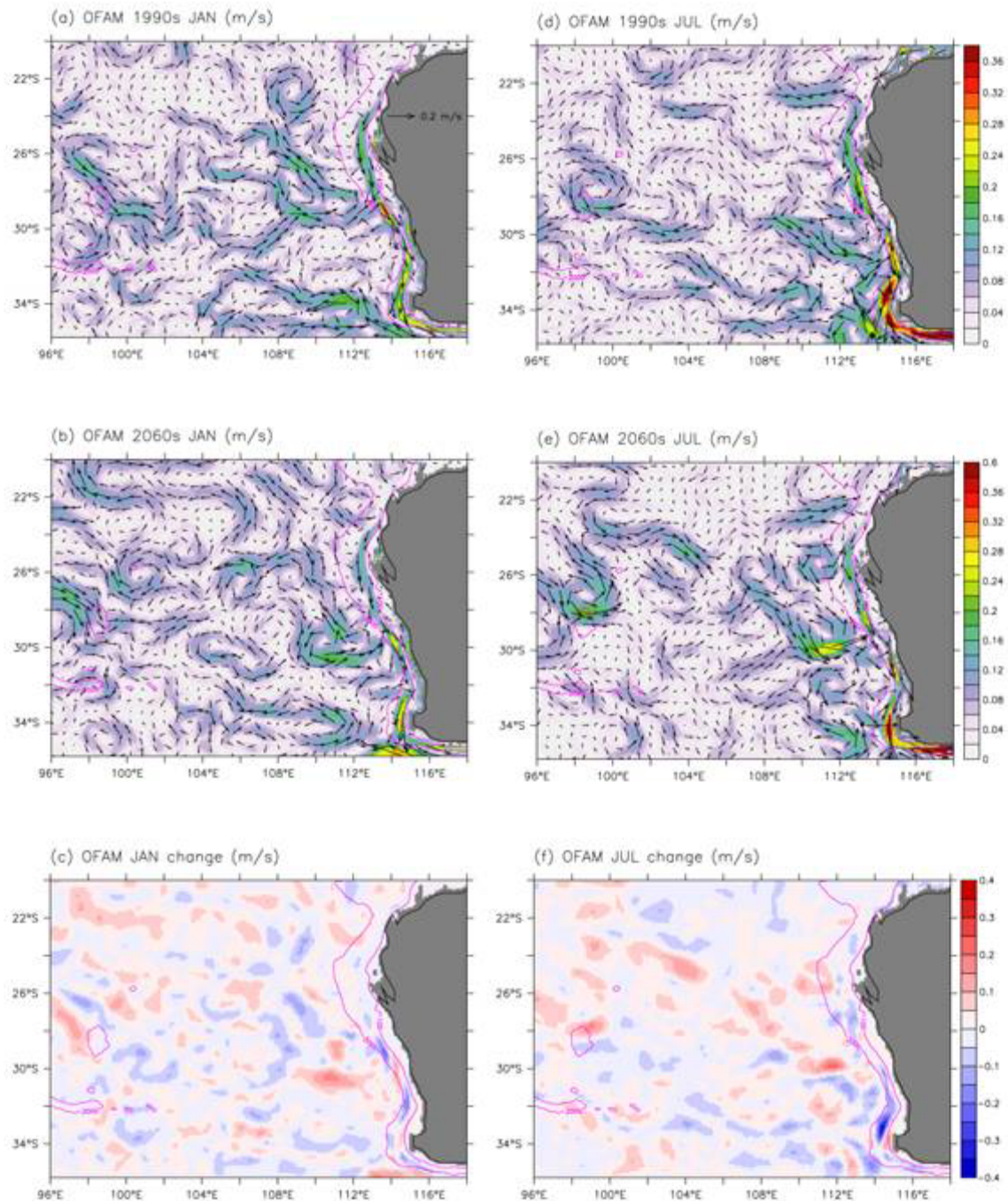


Figure 6: OFAM time-mean circulation off Western Australia from CTRL (left) and FUTR (center).

Colors show the magnitude of currents (depth-averaged over 0–200 m) in m/s. Vector lengths correspond to velocity magnitude, scale shown in (a). (c, f): Velocity difference in January (c) and July (f) between the two time slices of 2060s and 1990s. The magenta lines indicate 100m and 2000m isobaths.

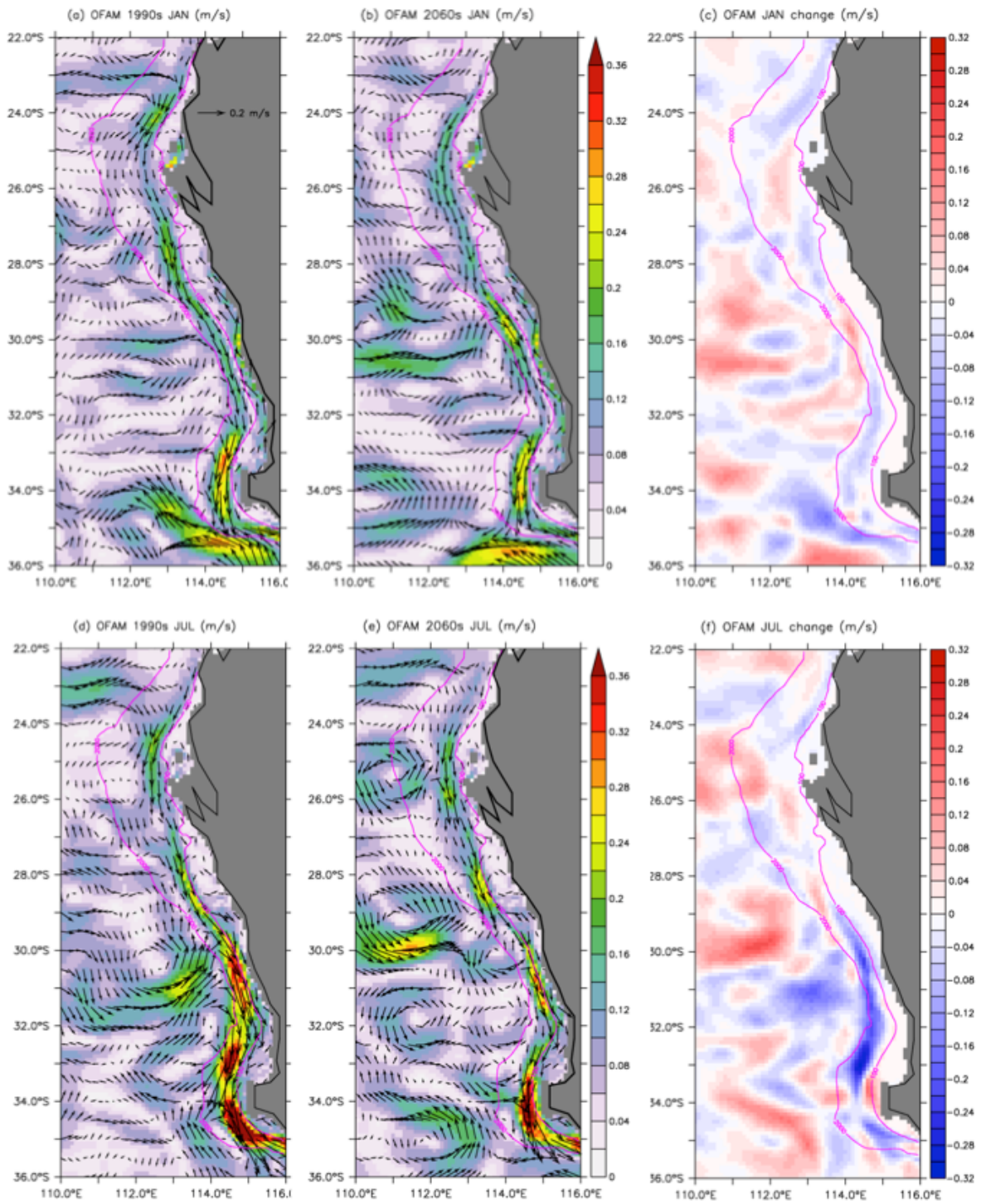


Figure 7: The same as Fig. 6, but for a zoomed view.

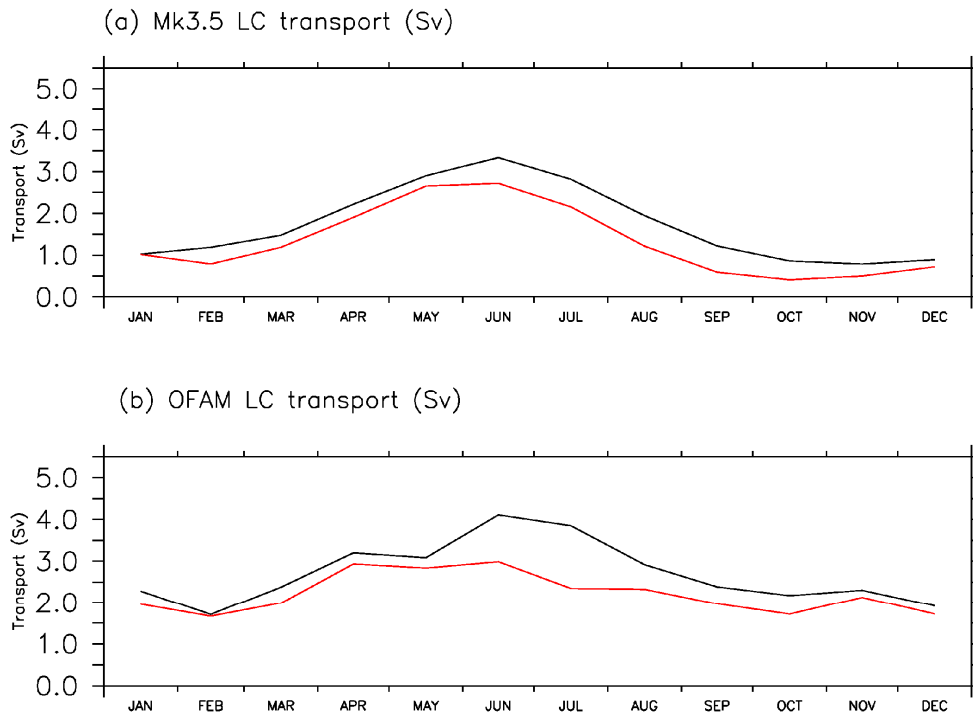


Figure 8: Seasonal cycle of the Leeuwin Current transport from (a) Mk3.5 and (b) OFAM (b): 1990s (black) and 2060s (red). Southward transport is positive. The Mk3.5 transport is estimated from southward flow averaged over 32° - 34° S (0-200m, coast to 108°). LC transport from OFAM is calculated from southward flow (0-200m, coast to 114° E) averaged over 32° - 34° S.

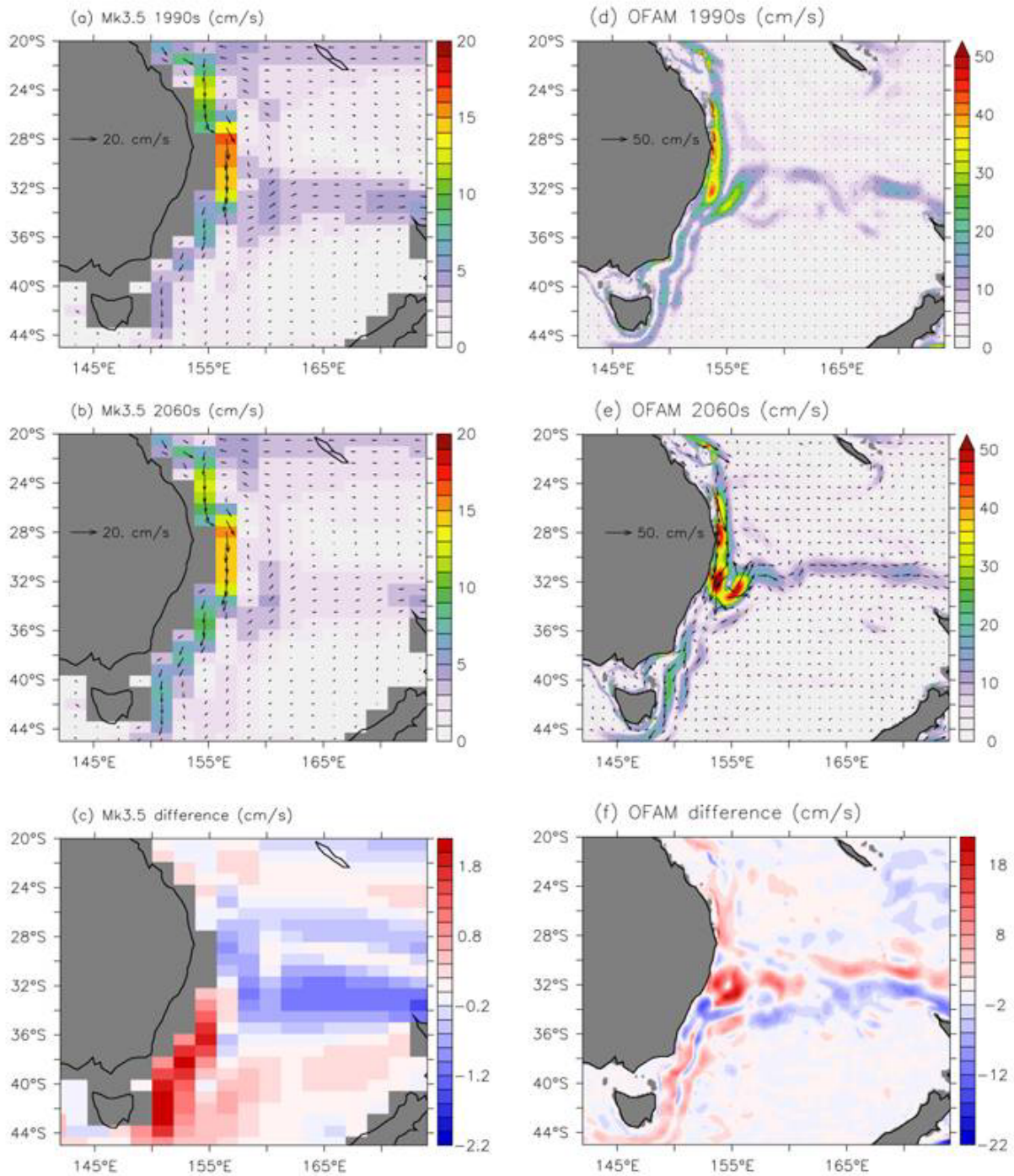


Figure 9: Time-mean circulation off the east coast of Australia from Mk3.5 (left) and OFAM (right) in the 1990s (top) and 2060s (center) and the differences between the two decades (bottom). Colors show current speed depth-averaged over 0–600 m in cm/s. Vector length represents current speed averaged over 0-600m in cm/s, and the corresponding vector scales are shown in (a-d). Note the scale in (f) is 10 times larger than (c).

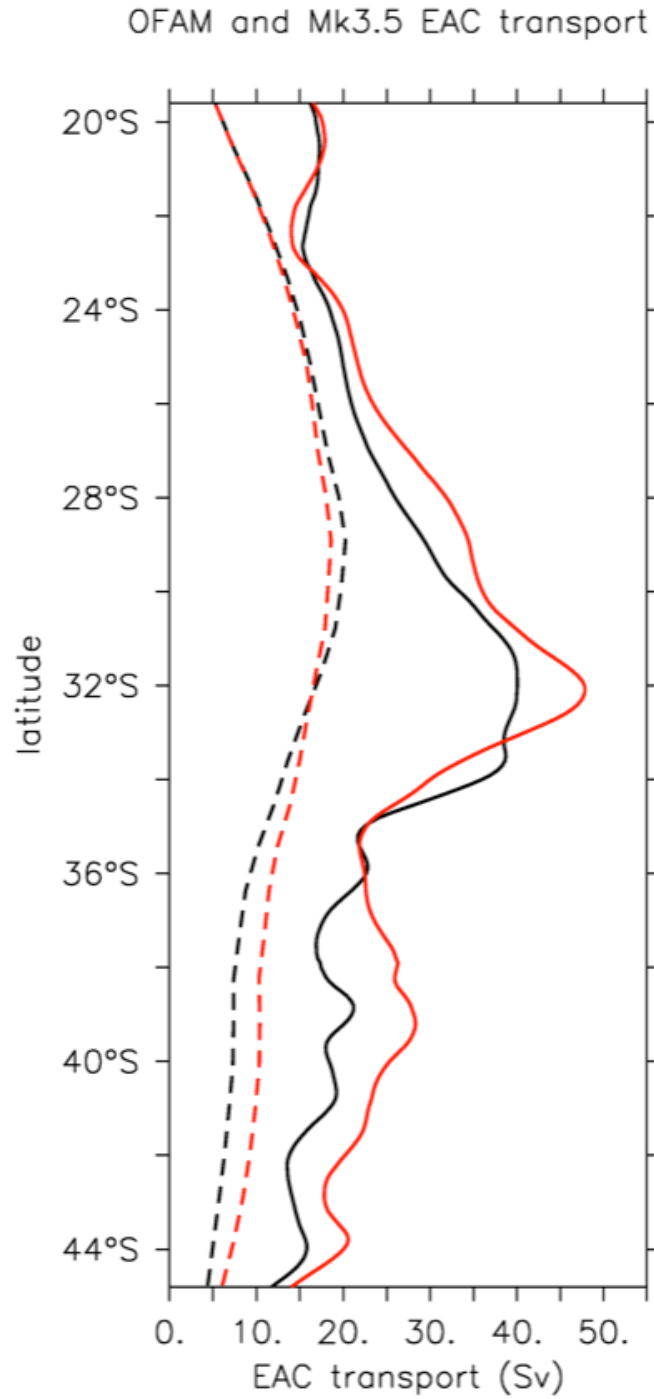


Figure 10: Annual-mean EAC transport along its path: Mk3.5 (dashed) and OFAM (solid). Red line is 2060s, black 1990s. Transport is calculated as depth-integrated southward flow from 148°E to 157°E, 0-600m.

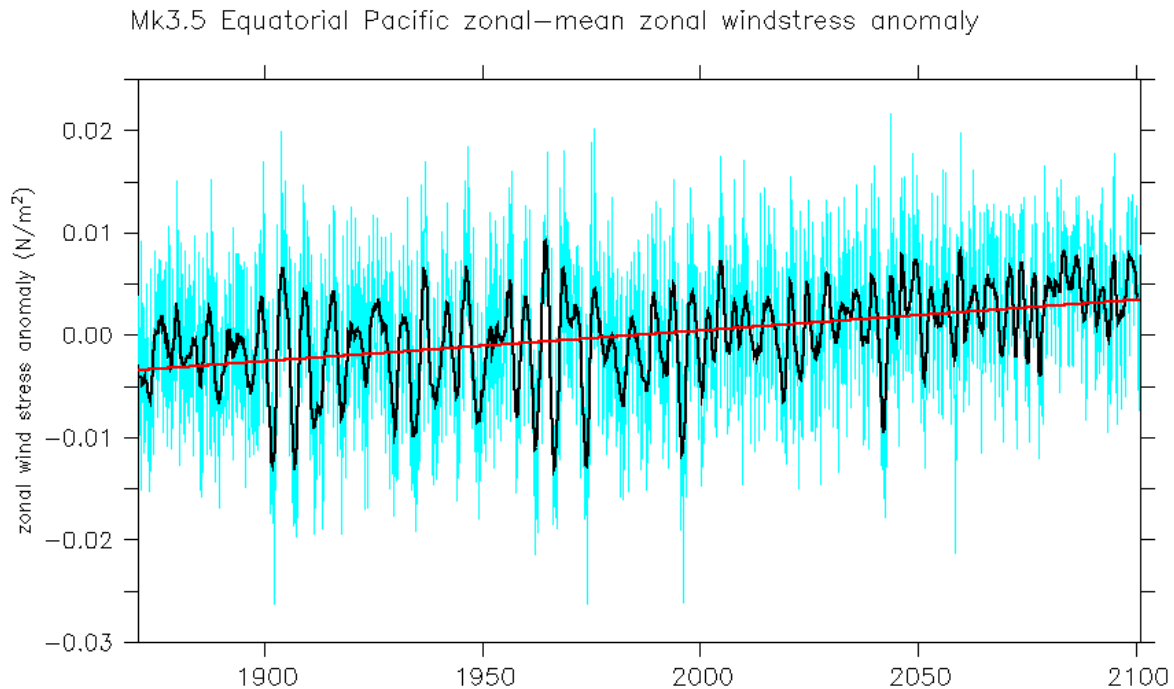


Figure 11: Equatorial Pacific zonal-mean zonal wind stress anomaly (N/m^2) from the Mk3.5 20C3M experiment (1860-2000) and SRES A1B (2001-2100) simulations. The zonal wind-stress anomaly is averaged 120°E – 70°W , 5°S – 5°N . The zonal wind-stress anomaly is averaged 120°E – 70°W , 5°S – 5°N . The cyan curve is the monthly mean, black line the annual mean, and red line the trend. Note that zonal windstress in the equatorial Pacific is westward (negative in this figure), so a positive anomaly indicates a weakening of windstress there. The monthly difference in the wind stress over the global domain from the two time slices (2060s and 1990s) is used to compute a 10-year averaged monthly climatology in the future forcing used in the downscaling experiments.

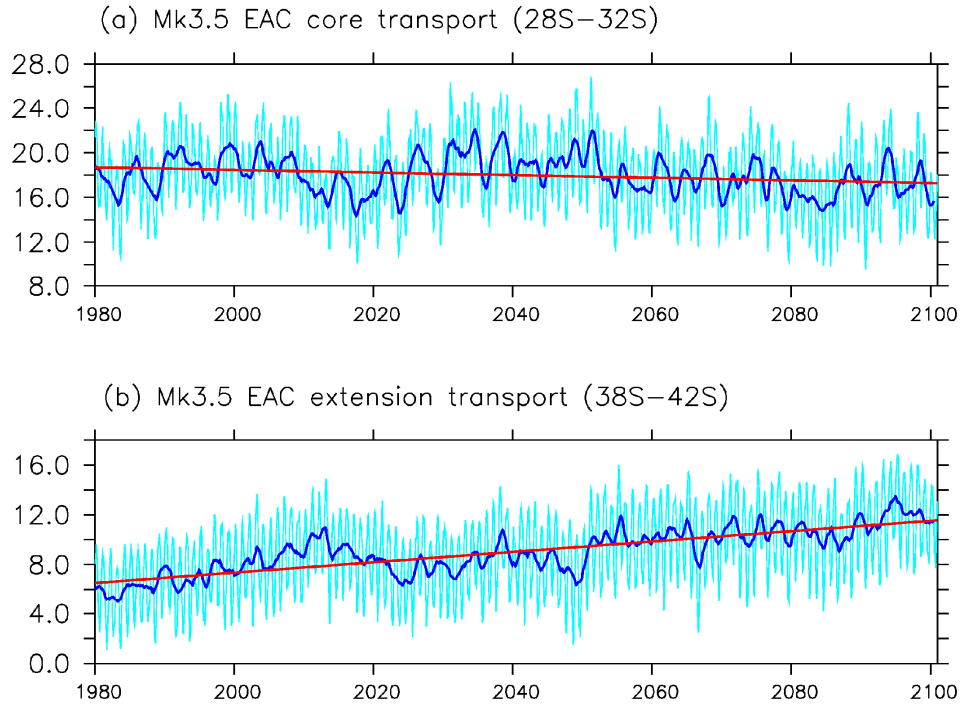


Figure 12: Mk3.5 EAC transport from 1980 to 2100. (a) EAC core transport averaged over 28°–32S; and (b) EAC extension transport (averaged over 38S–42°S). Mk3.5 transport is integrated from southward flows 148°E to 160°E, 0–600m. The cyan curve is the monthly mean, blue line the annual mean, and red line the trend.